



OPEN

SUBJECT AREAS:  
INFORMATION STORAGE  
FERROELECTRICS AND  
MULTIFERROICSReceived  
21 November 2013Accepted  
17 March 2014Published  
4 April 2014Correspondence and  
requests for materials  
should be addressed to  
Y.G.Z. (ygzhao@  
tsinghua.edu.cn)

# Bipolar loop-like non-volatile strain in the (001)-oriented $\text{Pb}(\text{Mg}_{1/3}\text{Nb}_{2/3})\text{O}_3\text{-PbTiO}_3$ single crystals

Lifeng Yang<sup>1,2</sup>, Yonggang Zhao<sup>1,2</sup>, Sen Zhang<sup>1,2,3</sup>, Peisen Li<sup>1,2</sup>, Ya Gao<sup>4</sup>, Yuanjun Yang<sup>5</sup>, Haoliang Huang<sup>5</sup>, Peixian Miao<sup>1,2</sup>, Yan Liu<sup>1,2</sup>, Aitian Chen<sup>1,2</sup>, C. W. Nan<sup>4</sup> & Chen Gao<sup>5</sup>

<sup>1</sup>Department of Physics and State Key Laboratory of Low-Dimensional Quantum Physics, Tsinghua University, Beijing 100084, P. R. China, <sup>2</sup>Collaborative Innovation Center of Quantum Matter, Beijing 100084, P. R. China, <sup>3</sup>College of Science, National University of Defense Technology, Changsha 410073, P. R. China, <sup>4</sup>State Key Laboratory of New Ceramics and Fine Processing, and Department of Materials Science and Engineering, Tsinghua University, Beijing 100084, P. R. China, <sup>5</sup>National Synchrotron Radiation Laboratory, University of Science and Technology of China, Hefei, Anhui 230026, P. R. China.

**Strain has been widely used to manipulate the properties of various kinds of materials, such as ferroelectrics, semiconductors, superconductors, magnetic materials, and “strain engineering” has become a very active field. For strain-based information storage, the non-volatile strain is very useful and highly desired.**

**However, in most cases, the strain induced by converse piezoelectric effect is volatile. In this work, we report a non-volatile strain in the (001)-oriented  $\text{Pb}(\text{Mg}_{1/3}\text{Nb}_{2/3})\text{O}_3\text{-PbTiO}_3$  single crystals and demonstrate an approach to measure the non-volatile strain. A bipolar loop-like S-E curve is revealed and a mechanism involving 109° ferroelastic domain switching is proposed. The non-volatile high and low strain states should be significant for applications in information storage.**

Strain has been widely used to manipulate the properties of various kinds of materials<sup>1–4</sup>, such as ferroelectrics<sup>1</sup>, semiconductors<sup>2</sup>, superconductors<sup>3</sup>, magnetic materials<sup>4</sup>, etc., and “strain engineering” has become a very active field<sup>1</sup>. One popular way to introduce strain is via lattice misfit between the epitaxial film and the substrate, and dramatic variation of strain can be realized by selecting suitable film and substrate<sup>1</sup>. However, in this case, the strain can not be tuned continuously and reversibly, and different substrates may induce other effects besides the strain effect when comparing the properties of films grown on different substrates. In this regard, converse piezoelectric effect is very useful for introducing continuous and reversible strain by electric fields. Recently the strain-mediated multiferroic heterostructures, composed of magnetic thin films and ferroelectrics (FE), have attracted much attention due to the magnetoelectric coupling between magnetic thin films and FE<sup>5–14</sup>. In these multiferroic heterostructures, strain is produced via the converse piezoelectric effect of FE and can be modulated continuously and reversibly. This kind of strain becomes a primary pathway to control the electronic transport and magnetic properties of the magnetic films in the multiferroic heterostructures, and “straintronics” has been proposed<sup>15</sup>. Owing to the superior piezoelectric properties<sup>16</sup>, relaxor ferroelectrics such as  $(1-x)\text{Pb}(\text{Mg}_{1/3}\text{Nb}_{2/3})\text{O}_3\text{-xPbTiO}_3$  (PMN-PT) single crystals, which are binary solid solution system ( $x$  represents the nominal composition of  $\text{PbTiO}_3$ ), have been widely used in the strain-mediated multiferroic heterostructures, besides their applications in ultrasonic devices, telecommunication, medical imaging<sup>17</sup>. So far, most reported in-plane strain-electric field (S-E) behavior of the (001)-oriented PMN-PT is a symmetric butterfly-like curve without remanent strain<sup>18</sup>, i.e. the electric-field induced strain is volatile. However, non-volatile strain is more important and highly desired for the strain-based information storage in the multiferroic heterostructures<sup>19</sup>. For electric-field induced reversible non-volatile strain, there are only a few reports on FE materials with remnant strain states in the S-E curves, which can be classified into two types. For type I, the polarization-electric field (P-E) hysteresis loop is offset about the origin as shown in polycrystalline  $\text{PbZr}_{1-x}\text{Ti}_x\text{O}_3$  due to an internal field which is generated by different kinds of defects<sup>20</sup>. Because the correlation between strain and polarization, the S-E curves also deviate from the symmetric butterfly-like curves and show an asymmetric behavior. In this case, there is indeed remanent strain at zero electric field, but the asymmetric behavior of the butterfly-like curves are deter-

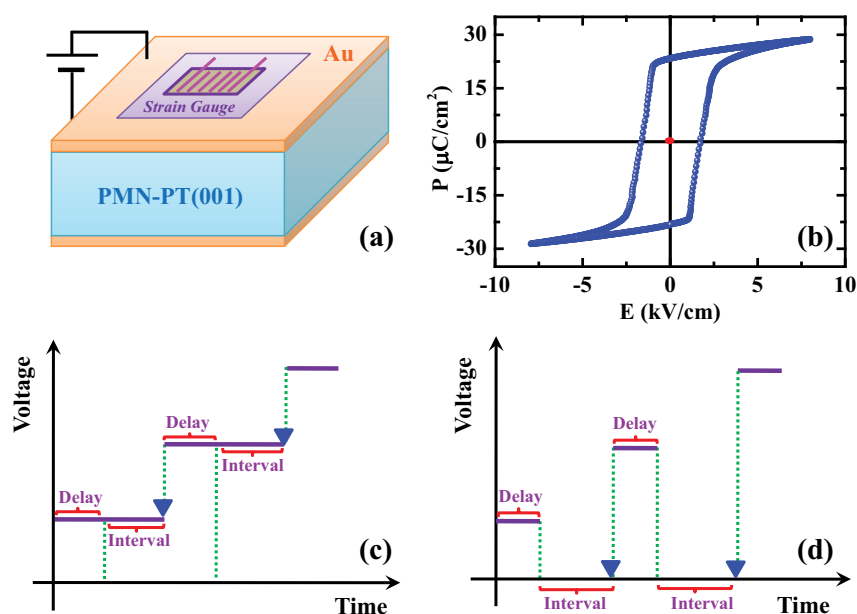


**Figure 1 | Experimental configuration, ferroelectric property and two different methods for measuring strain.** (a) Schematic of the sample and the experimental configuration. (b) P-E loop of PMN-PT. (c) and (d) Schematic of the continuous and pulsed measurement methods for S-E curves, respectively. The strain measurement starts at the end of interval as pointed by the solid blue triangle symbols.

mined by the polarity of the space charges<sup>21</sup>, accompanied with fatigue<sup>22,23</sup>. For type II, Wu *et al.*<sup>24–26</sup> recently obtained the remanent strain in the (011)-oriented PMN-PT single crystals. When a critical reversed electric field was applied, the polarizations reoriented to the four possible in-plane  $\langle 111 \rangle$  directions, which acted as a metastable state during the polarization reversal process. After decreasing the electric field to zero, hysteresis occurred for both P-E and S-E curves and two different strain states arise. However, a critical reversed electric field is required to induce the effect in these systems. If the electric fields applied to PMN-PT are larger or smaller than the critical field, the remanent strain will decrease dramatically<sup>24</sup>. Since the critical reversed electrical field is a bit smaller than the coercive field, the cycle of the electric field applied to the (011)-oriented PMN-PT is actually unipolar as mentioned in Wu's paper<sup>24</sup>, while for the bipolar case, there is no remanent strain<sup>24</sup>. In this paper, we report a non-volatile strain in the (001)-oriented PMN-PT single crystals. A bipolar loop-like S-E curve is revealed and a mechanism involving  $109^\circ$  ferroelastic domain switching is proposed. We also put forward and demonstrate an approach for measuring the non-volatile strain.

## Results

**Methods for strain measurement and loop-like strain behaviors in PMN-PT single crystals.** Figure 1a is the schematic of the sample and the experimental configuration. (001)-oriented (1-x)PMN-xPT ( $x = 0.28$ , PMN-PT with 28% of PT) single crystals were used in our work. The single crystal orientation and microstructure of the polished surface were characterized as shown in Fig. S1 in Supplementary Information. Figure 1b shows the P-E hysteresis loop for PMN-PT measured by using a Radiant Technologies Precision Premier II system. The in-plane S-E curves were measured by using the continuous method as shown in Figure 1c, which has been commonly used in the literature<sup>17,18</sup>. We measured the in-plane strains along the [110] and [1-10] directions of the (001) plane, whose converse piezoelectric responses are more sensitive<sup>27</sup>. The S-E curve along the [110] direction is shown in Figure 2a. In contrast to the normal symmetric butterfly-like curve<sup>18</sup>, it shows an asymmetric behavior with two remanent strain states at zero electric field. The in-plane S-E curve along the perpendicular direction [1-10] also shows an asymmetric butterfly-like behavior (Figure S2

in Supplementary Information) and is complementary with that of the [110] direction, providing a clue to the origin of the phenomenon as discussed later.

As shown in Fig. 1b, the hysteresis loop of our sample is symmetric about the origin, which means that the internal field induced by defects is negligible. This is different from the aforementioned type I asymmetric S-E curve, which is related to the asymmetry of the P-E hysteresis loop. Moreover, unlike the unipolar S-E curves for the aforementioned type II<sup>24</sup>, the S-E curve of our sample is bipolar. In addition, the electric fields applied in our work ( $\pm 8$  kV/cm) are much higher than the coercive field (1.2 kV/cm) characterized in the P-E loop (Fig. 1b). So the sample is in the saturated polarization states, which is different from the aforementioned type II case. Thus, a different mechanism for the asymmetry of S-E curves should be involved in our samples.

In order to get the non-volatile part in the asymmetric butterfly-like curves, we proposed an approach as shown in Fig. 1d, which is denoted as the pulsed measurements method. The detailed descriptions for the continuous and pulsed measurements are in the experimental section. In both measurements, we begin to measure the strain at the end of the interval. The difference is that electric voltage is always applied to the sample in the continuous measurement, while no electric voltage during the interval for the pulsed measurement. Thereby, in the pulsed measurement, the strain is measured at zero electric field and reflects the remanent strain. Figure 2b shows the S-E curve obtained by the pulsed measurement. Interestingly, it exhibits a bipolar loop-like behavior, similar to the P-E hysteresis loop (Fig. 1b). The loop-like S-E curve suggests that one can easily control the strain states by electric fields. For the perpendicular [1-10] direction, we also got the asymmetric butterfly-like and loop-like S-E curves (Fig. S2), which exhibit a reverse behavior compared to those of the [110] direction. Figure 2c shows the S-E curve obtained by subtracting the strain values in the loop-like curve (Fig. 2b) from those in the asymmetric butterfly-like curve (Fig. 2a) at the same voltage point by point. The S-E curve in Fig. 2c is a symmetric butterfly-like curve, which is common in the previous reports<sup>18</sup>. Similar results were also obtained along the [1-10] direction (Fig. S2). Based on the above results and analyses, it can be deduced that the observed asymmetric butterfly-like S-E curves are

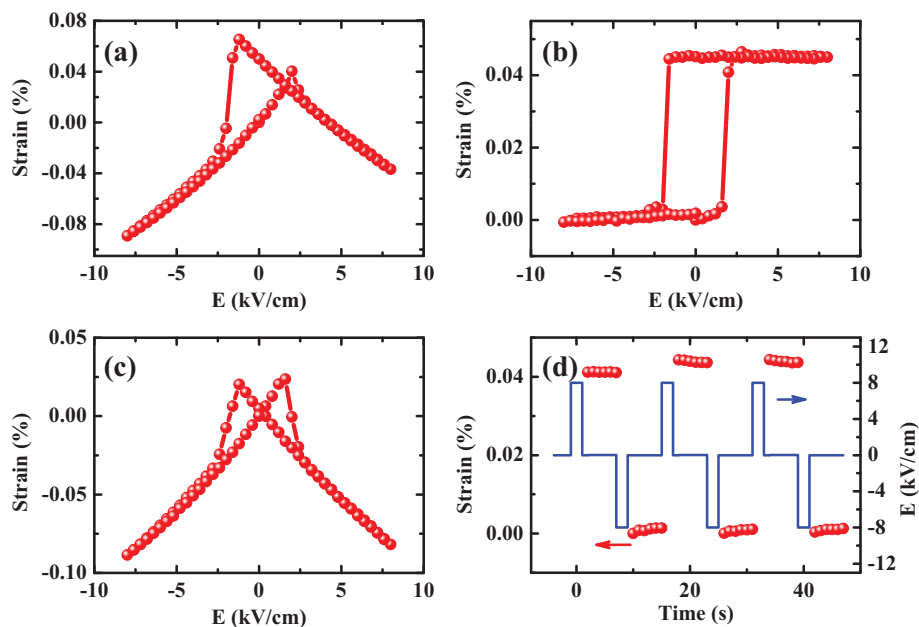


**Figure 2 | Electric-field tuned strain behavior along [110] direction.** (a) and (b) S-E curves along the [110] direction measured by continuous and pulsed measurements, respectively. (c) The curve obtained by subtracting the strain values in the loop-like S-E curves (Figure 2b) from those in asymmetric butterfly curves (Figure 2a). (d) The stable and remarkable high/low remanent strain states achieved by switching the polarity of the pulsed electric field.

composed of the symmetric butterfly-like and the loop-like curves. Stable and remarkable high/low remanent strain states can be achieved by switching the polarities of the pulsed electric fields as shown in Fig. 2d for the [110] direction and Fig. S2d for the [1-10] direction. It can be seen that the pulsed electric field polarity dependence of the high/low strain states for these two directions is converse, which is consistent with the complementary behavior in their S-E curves (Fig. 2 and Fig. S2). Instead of a specific value or range of electric field required in the type II case, any fields larger than the coercive field of the sample can induce the remarkable high/low non-volatile strain states. Moreover, as the sample is in the saturated polarization states, the non-volatile strain states were stable and didn't show an obvious relaxation with time, which is in contrast to the behavior of the (011)-oriented PMN-PT<sup>28</sup>. And the high/low strain states can be switched by pulsed electric fields for thousands of times without obvious fatigue effect (Fig. S3 in Supplementary Information).

**Proportions of ferroelastic switching in PMN-PT single crystals with different S-E behaviors.** It should be mentioned that not all the samples exhibit the asymmetric butterfly-like S-E curves. We also obtained the symmetric butterfly-like curve as shown in Fig. S4a in Supplementary Information, similar to that reported by Thiele<sup>18</sup>, in samples with the same nominal composition as those showing the asymmetric butterfly-like behavior. Figure S4b shows the S-E curves measured by the pulsed measurement. Obviously, there is no remanent strain at zero field in this kind of samples. Hereafter, we denote the samples with the asymmetric and symmetric S-E curves as sample A and sample S, respectively. To identify the differences between these two kinds of samples, we carried out XRD-RSM with in situ electric fields since it can provide straightforward information on the microstructure of the samples and the switching category of FE domains. PMN-PT samples are in the rhombohedral phase with eight spontaneous polarizations along the  $\langle 111 \rangle$  directions, denoted as  $r1^+/r1^-$ ,  $r2^+/r2^-$ ,  $r3^+/r3^-$ ,  $r4^+/r4^-$  as shown in Fig. 3a and 3b. When the polarity of electric field was changed, the spontaneous polarizations can be switched by  $71^\circ$ ,  $109^\circ$  and  $180^\circ$ , respectively. Polarization variants changing from

$r1^+/r3^+$  to  $r2^-/r4^-$  or  $r2^+/r4^+$  to  $r1^-/r3^-$  (vice versa) correspond to the  $109^\circ$  switching, while polarization variants changing from  $r1^+$  to  $r3^-$  or  $r3^+$  to  $r1^-$  (the same case for  $r2/r4$ ) correspond to the  $71^\circ$  switching, and polarization variants without any category change (e.g.  $r1^+$  to  $r1^-$  and so on) correspond to the  $180^\circ$  switching. Figure 3c and 3d show the reflections around the (113) peak for sample A under  $-8$  kV/cm and  $+8$  kV/cm, respectively. The distortions corresponding to polarization variants  $r2$  and  $r4$  are

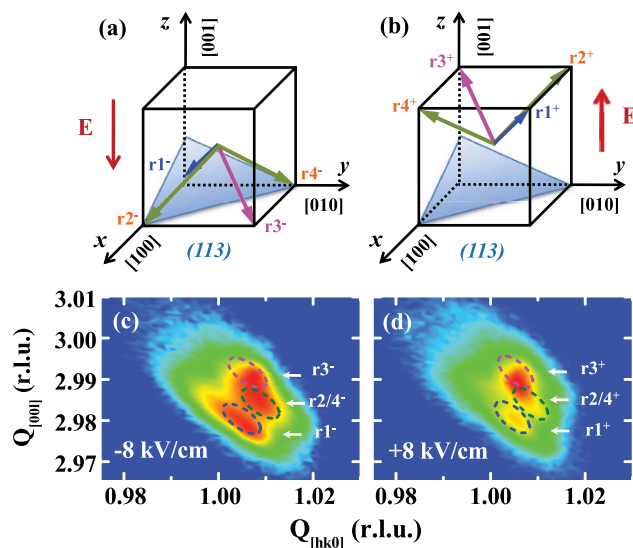


**Figure 3 | The schematic diagram of the polarization variants and XRD-RSMs around (113) reflections.** (a) and (b) Configurations of the (113) crystal face (translucent light blue plane) and polarization variants of rhombohedral phase under negative and positive electric fields, respectively. (c) and (d) (113) reflection peak of XRD-RSMs for sample A with in situ electric fields of  $-8$  kV/cm and  $+8$  kV/cm, respectively. Ellipses with different colors in RSMs outline the contours of the deduced spots.



**Table 1** | Proportions of different polarization variants under positive and negative electric fields, respectively

$E$ (kV/cm)	$r1$	$r2/r4$	$r3$	Correlation Coefficient
-8	41.7%	55.5%	2.8%	0.96
+8	17.1%	35.6%	47.3%	0.94

degenerate in the (113) reflection peak, so there are three spots corresponding to  $r1$ ,  $r3$ , and  $r2/r4$ , respectively. According to the lattice parameters in the rhombohedral structure<sup>29</sup> and the analytical method<sup>30</sup>, we analyzed the positions and intensities of the spots (see SI for details), which can give the percentages of different polarization variants under positive and negative electric fields, respectively. Table 1 shows the results for sample A, suggesting that the proportion of  $r2/r4$  under +8 kV/cm is about 20% less than that under -8 kV/cm. Since the change between  $r2/r4$  and  $r1/r3$  from positively poled cases to negatively poled cases (vice versa) corresponds to the  $109^\circ$  switching, the 20% reduction of  $r2/r4$  proportion represents the net proportion of  $109^\circ$  switching. For comparison, we also measured the reflections around the (113) peak with in situ electric fields for sample S. The results are shown in Figure S4c and S4d. Similar to sample A, the (113) reflection peak also shows three spots. We analyzed the data using the same method as for sample A and the results are shown in Table S1. The percentages of different polarization variants are almost unchanged with the polarities of electric field. This means that there are  $71/180^\circ$  switching, but almost no net  $109^\circ$  switching since the percentage of  $r2/r4$  is nearly unchanged under positive and negative electric fields.

**The crucial role of the net  $109^\circ$  switching for the non-volatile strain.** In sample A, there are not only  $71/180^\circ$  switching but also about 20% of net  $109^\circ$  switching. While in sample S, there are only  $71/180^\circ$  switching and almost no net  $109^\circ$  switching. Combined with the complementary property in the loop-like curves in sample A (Fig. 2b and S2b) and the symmetric butterfly-like curves in sample S (Fig. S4a), it can be concluded that the loop-like S-E curve is related to the net  $109^\circ$  switching. In contrast, without net

$109^\circ$  switching, the S-E curve exhibits the butterfly-like behavior. Figure 4 is the schematic diagram of the  $109^\circ$  switching,  $71/180^\circ$  switching and corresponding changes of distortion/strain. For polarization switching from  $P^+$  to  $P^-$ , we take  $r1^+$  and  $r3^+$  as an example to show the  $109^\circ$  switching (right) and  $71/180^\circ$  switching (left) as shown in the upper panel of Fig. 4. It can be seen that the projections of polarizations to the (001) plane before and after the  $109^\circ$  switching are perpendicular, while they are parallel before and after the  $71/180^\circ$  switching. As a result, the in-plane tensile distortions related to the polarizations are perpendicular before and after the  $109^\circ$  switching and parallel before and after the  $71/180^\circ$  switching (lower panel of Fig. 4). It is also noted that change of the tensile distortions along the [110] and [1-10] directions are complementary for the  $109^\circ$  switching. This is the origin of the complementary loop-like curves of sample A along the two perpendicular directions. In sample S, there are only  $71/180^\circ$  switching and the S-E curves show a symmetric butterfly-like behavior without remanent strain.

## Discussion

An interesting question arises as why sample A and sample S, with the same nominal composition, show such a big difference in the S-E curves, related to the presence and absence of net  $109^\circ$  switching in sample A and sample S, respectively. It is likely that defects/defect configurations in the crystals may play an important role. As reported by Fu *et al.*<sup>31</sup>, polarization rotation along the different paths needs to overcome different energy barriers. And it has been shown that defects can strongly affect the barrier for polarization rotation, e. g. defects make the  $180^\circ$  polarization flip become a feasible process<sup>32</sup>. It was also shown that defect configurations play an important role in the polarization switching<sup>33</sup>. These may shed light on our case as follows. Some defects/defect configurations in sample A lowers the energy barrier between the two polarization configurations with the polar axis rotating by  $109^\circ$ , which is crucial for the loop-like S-E curves. In contrast, it is not the case for sample S and  $109^\circ$  domain switching is not favored due to the required high energy. The presence of key defects/defect configurations may be due to details during the crystal growth process. Further study on this issue is deserved.

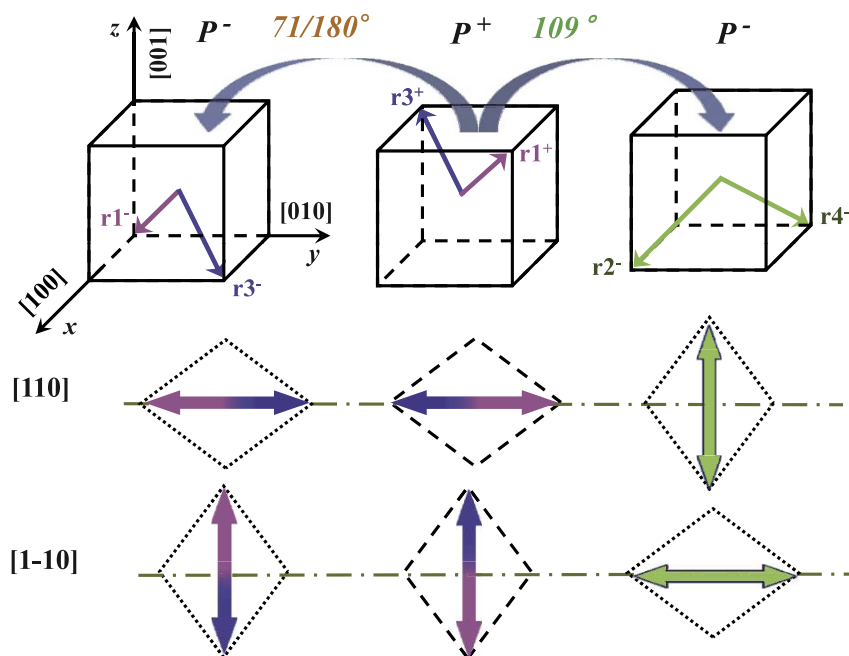


**Figure 4** | Correlation between domain switching and distortion. Schematic diagrams of the  $109^\circ$  switching,  $71/180^\circ$  switching (upper panel) and corresponding changes of distortion (lower panel).





In conclusion, we report a non-volatile strain in the (001)-oriented PMN-PT single crystals. A bipolar loop-like S-E curve is revealed and a mechanism involving  $109^\circ$  ferroelastic domain switching is proposed. We also put forward and demonstrate an approach for measuring the non-volatile strain. As a comparison, the non-volatile strain in the (011)-oriented PMN-PT reported previously is dependent on a critical reversed electric field and decreases dramatically if the electric field deviates from the critical value. While the non-volatile strain in the (001)-oriented PMN-PT in our work can be obtained by any fields larger than the coercive field and maintains a stable state. The non-volatile high and low strain states should be significant for applications in information storage.

## Methods

Our samples are one-side-polished (001)-oriented PMN-PT with the edges cut along the pseudocubic [110] and [1-10] directions, and dimensions of  $5\text{ mm} \times 5\text{ mm} \times 0.5\text{ mm}$ . Au layers of 100 nm thick were deposited on both sides of the samples as electrodes. The strain gauge was pasted on the sample surface with glue M-Bond 610, and kept at  $120^\circ\text{C}$  for 2 h to strengthen the paste effect.

Two kinds of measurements for S-E curves are shown in Fig. 1c and 1d, which are named as continuous and pulsed measurements, respectively. In the continuous measurement, the voltage applied to the sample is increased with a step of 20 V. After a period of delay, an interval is followed. At the end of the interval, the measurement begins, and then the voltage is changed for the next cycle. So the voltage is always applied. In the pulsed measurement, the voltage is also increased with a step of 20 V. After a period of delay, the voltage is removed for an interval. At the end of the interval, the strain measurement starts. After that the voltage is changed and the measurement goes into the next cycle. We carried out the XRD-RSM experiments with in situ electric fields of  $\pm 8\text{ kV/cm}$  using the synchrotron radiation x-ray source. All the measurements were carried out at room temperature.

- Schlom, D. G. *et al.* Strain tuning of ferroelectric thin films. *Annu. Rev. Mater. Res.* **37**, 589–626 (2007).
- Chu, M., Sun, Y. K., Aghoram, U. & Thompson, S. E. Strain: A Solution for Higher Carrier Mobility in Nanoscale MOSFETs. *Annu. Rev. Mater. Res.* **39**, 203–229 (2009).
- Locquet, J. P. *et al.* Doubling the critical temperature of  $\text{La}_{1.9}\text{Sr}_{0.1}\text{CuO}_4$  using epitaxial strain. *Nature* **394**, 453–456 (1998).
- Van Tendeloo, G., Lebedev, O. I., Hervieu, M. & Raveau, B. Structure and microstructure of colossal magnetoresistant materials. *Rep. Prog. Phys.* **67**, 1315–1365 (2004).
- Yang, J. J. *et al.* Electric field manipulation of magnetization at room temperature in multiferroic  $\text{CoFe}_2\text{O}_4/\text{Pb}(\text{Mg}_{1/3}\text{Nb}_{2/3})_{0.7}\text{Ti}_{0.3}\text{O}_3$  heterostructures. *Appl. Phys. Lett.* **94**, 212504 (2009).
- Chen, Y. J. *et al.* Large converse magnetoelectric coupling in FeCoV/lead zinc niobate-lead titanate heterostructure. *Appl. Phys. Lett.* **94**, 082504 (2009).
- Geprägs, S., Brandmaier, A., Opel, M., Gross, R. & Goennenwein, S. T. B. Electric field controlled manipulation of the magnetization in Ni/BaTiO<sub>3</sub> hybrid structures. *Appl. Phys. Lett.* **96**, 142509 (2010).
- Liu, M. *et al.* Giant Electric Field Tuning of Magnetic Properties in Multiferroic Ferrite/Ferroelectric Heterostructures. *Adv. Funct. Mater.* **19**, 1826–1831 (2009).
- Chen, Q. P. *et al.* Electric-field control of phase separation and memory effect in  $\text{Pr}_{0.6}\text{Ca}_{0.4}\text{MnO}_3/\text{Pb}(\text{Mg}_{1/3}\text{Nb}_{2/3})_{0.7}\text{Ti}_{0.3}\text{O}_3$  heterostructures. *Appl. Phys. Lett.* **98**, 172507 (2011).
- Thiele, C. *et al.* Voltage-controlled epitaxial strain in  $\text{La}_{0.7}\text{Sr}_{0.3}\text{MnO}_3/\text{Pb}(\text{Mg}_{1/3}\text{Nb}_{2/3})_{0.3}\text{O}_3\text{-PbTiO}_3(001)$  films. *Appl. Phys. Lett.* **87**, 262502 (2005).
- Wang, Z. G., Yang, Y. D., Viswan, R., Li, J. F. & Viehland, D. Giant electric field controlled magnetic anisotropy in epitaxial  $\text{BiFeO}_3\text{-CoFe}_2\text{O}_4$  thin film heterostructures on single crystal  $\text{Pb}(\text{Mg}_{1/3}\text{Nb}_{2/3})_{0.7}\text{Ti}_{0.3}\text{O}_3$  substrate. *Appl. Phys. Lett.* **99**, 043110 (2011).
- Hsu, C. J., Hockel, J. L. & Carman, G. P. Magnetoelectric manipulation of domain wall configuration in thin film  $\text{Ni}[\text{Pb}(\text{Mn}_{1/3}\text{Nb}_{2/3})_{0.68}\text{-}[\text{PbTiO}_3]_{0.32}$  (001) heterostructure. *Appl. Phys. Lett.* **100**, 092902 (2012).
- Zhang, S. *et al.* Electric-Field Control of Nonvolatile Magnetization in  $\text{Co}_{40}\text{Fe}_{40}\text{B}_{20}/\text{Pb}(\text{Mg}_{1/3}\text{Nb}_{2/3})_{0.7}\text{Ti}_{0.3}\text{O}_3$  Structure at Room Temperature. *Phys. Rev. Lett.* **108**, 137203 (2012).
- Eerenstein, W., Wiora, M., Prieto, J. L., Scott, J. F. & Mathur, N. D. Giant sharp and persistent converse magnetoelectric effects in multiferroic epitaxial heterostructures. *Nat. Mater.* **6**, 348–351 (2007).
- Roy, K., Bandyopadhyay, S. & Atulasimha, J. Hybrid spintronics and straintronics: A magnetic technology for ultra low energy computing and signal processing. *Appl. Phys. Lett.* **99**, 063108 (2011).
- Service, R. F. Shape-changing crystals get shifter. *Science* **275**, 1878 (1997).
- Park, S. E. & Shrout, T. R. Ultrahigh strain and piezoelectric behavior in relaxor based ferroelectric single crystals. *J. Appl. Phys.* **82**, 1804–1811 (1997).
- Thiele, C., Dörr, K., Bilani, O., Rödel, J. & Schultz, L. Influence of strain on the magnetization and magnetoelectric effect in  $\text{La}_{0.7}\text{A}_{0.3}\text{MnO}_3/\text{PMN-PT}(001)$  ( $A = \text{Sr,Ca}$ ). *Phys. Rev. B* **75**, 054408 (2007).
- Nan, T. X. *et al.* Voltage impulse induced bistable magnetization switching in multiferroic heterostructures. *Appl. Phys. Lett.* **100**, 132409 (2012).
- Lupascu, D. C. & Rödel, J. Fatigue in bulk lead zirconate titanate actuator materials. *Adv. Eng. Mater.* **7**, 882–898 (2005).
- Yu, L., Yu, S. W. & Feng, X. Q. Effects of electric fatigue on the butterfly curves of ferroelectric ceramics. *Mater. Sci. Eng. A* **459**, 273–277 (2007).
- Lupascu, D. C. & Verdier, C. Fatigue anisotropy in lead-zirconate-titanate. *J. Eur. Ceram. Soc.* **24**, 1663–1667 (2004).
- Weitzing, H., Schneider, G. A., Steffens, J., Hammer, M. & Hoffmann, M. J. Cyclic fatigue due to electric loading in ferroelectric ceramics. *J. Eur. Ceram. Soc.* **19**, 1333–1337 (1999).
- Wu, T. *et al.* Domain engineered switchable strain states in ferroelectric (011)  $[\text{Pb}(\text{Mg}_{1/3}\text{Nb}_{2/3})_{0.7}\text{Ti}_{0.3}\text{O}_3](1-x)\text{-}[\text{PbTiO}_3]x$  (PMN-PT,  $x \approx 0.32$ ) single crystals. *J. Appl. Phys.* **109**, 124101 (2011).
- Wu, T. *et al.* Electrical control of reversible and permanent magnetization reorientation formagnetoelectric memory devices. *Appl. Phys. Lett.* **98**, 262504 (2011).
- Liu, M. *et al.* Voltage-Impulse-Induced Non-Volatile Ferroelastic Switching of Ferromagnetic Resonance for Reconfigurable Magnetolectric Microwave Devices. *Adv. Mater.* **25**, 4886–4892 (2013).
- Davis, M., Damjanovic, D., Hayem, D. & Setter, N. Domain engineering of the transverse piezoelectric coefficient in perovskite ferroelectrics. *J. Appl. Phys.* **98**, 014102 (2005).
- Zhang, S. *et al.* Giant electrical modulation of magnetization in  $\text{Co}_{40}\text{Fe}_{40}\text{B}_{20}/\text{Pb}(\text{Mg}_{1/3}\text{Nb}_{2/3})_{0.7}\text{Ti}_{0.3}\text{O}_3(011)$  heterostructure. *Sci. Rep.* **4**, 3727 (2014).
- Noheda, B., Cox, D. E., Shirane, G., Gao, J. & Ye, Z. G. Phase diagram of the ferroelectric relaxor  $(1-x)\text{PbMg}_{1/3}\text{Nb}_{2/3}\text{O}_3\text{-xPbTiO}_3$ . *Phys. Rev. B* **66**, 054104 (2002).
- Baek, S. H. *et al.* Ferroelastic switching for nanoscale non-volatile magnetoelectric devices. *Nat. Mater.* **9**, 309–314 (2010).
- Fu, H. X. & Cohen, R. E. Polarization rotation mechanism for ultrahigh electromechanical response in single-crystal piezoelectrics. *Nature* **403**, 281–283 (2000).
- Kimmel, A. V., Weaver, P. M., Cain, M. G. & Sushko, P. V. Defect-Mediated Lattice Relaxation and Domain Stability in Ferroelectric Oxides. *Phys. Rev. Lett.* **109**, 117601 (2012).
- Noguchi, Y. J., Miwa, I., Goshima, Y. & Miyayama, M. Defect control for large remanent polarization in bismuth titanate ferroelectrics doping effect of higher-valent cations. *Jpn. J. Appl. Phys.* **39**, L1259–L1262 (2000).

## Acknowledgments

This work was supported by the 973 project of the Ministry of Science and Technology of China (Grant Nos. 2009CB929202 and 2009CB929203), National Science Foundation of China (Grant Nos. 10721404, 11179008 and 51332001), Special Fund of Tsinghua for basic research (Grant No. 201110810625) and Tsinghua National Laboratory for Information Science and Technology (TNList) Cross-discipline Foundation.

## Author contributions

L.Y. and Y.Z. planned the experiments. L.Y. made the samples and performed all the strain measurements with the assistance from S.Z., P.L., P.M., Y.G. and C.N. The data analysis was performed by L.Y., Y.L. and A.C. The XRD-RSM experiment and analysis were performed by Y.Y., H.H. and C.G. The paper was written by L.Y. and Y.Z. All authors reviewed and commented on the manuscript.

## Additional information

Supplementary information accompanies this paper at <http://www.nature.com/scientificreports>

Competing financial interests: The authors declare no competing financial interests.

How to cite this article: Yang, L.F. *et al.* Bipolar loop-like non-volatile strain in the (001)-oriented  $\text{Pb}(\text{Mg}_{1/3}\text{Nb}_{2/3})_{0.3}\text{-PbTiO}_3$  single crystals. *Sci. Rep.* **4**, 4591; DOI:10.1038/srep04591 (2014).



This work is licensed under a Creative Commons Attribution-NonCommercial-ShareAlike 3.0 Unported License. The images in this article are included in the article's Creative Commons license, unless indicated otherwise in the image credit; if the image is not included under the Creative Commons license, users will need to obtain permission from the license holder in order to reproduce the image. To view a copy of this license, visit <http://creativecommons.org/licenses/by-nc-sa/3.0/>